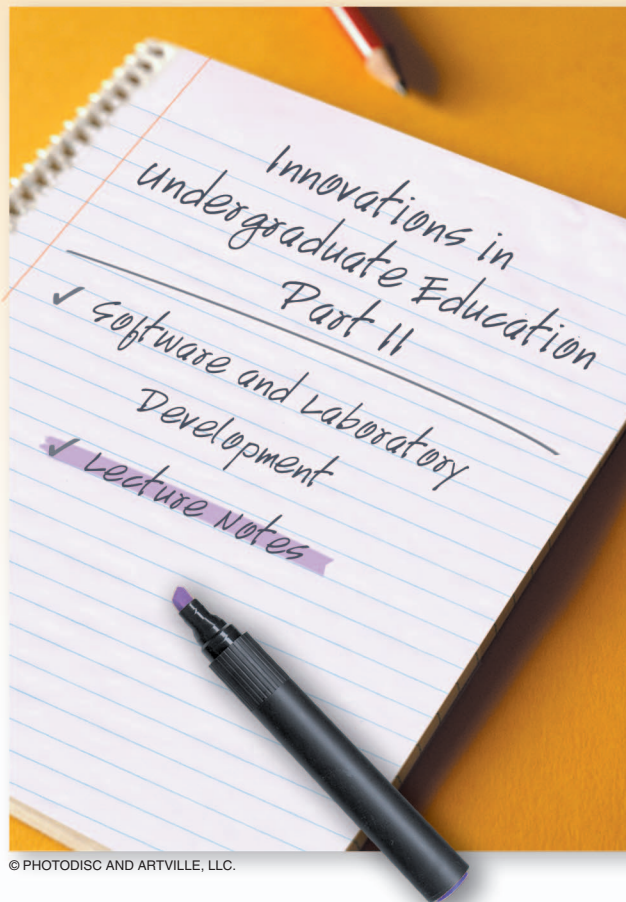


The Relation Between the 3-D Bode Diagram and the Root Locus

Insights into the connection between these classical methods



© PHOTODISC AND ARTVILLE, LLC.

Bode diagrams and root locus plots have been the cornerstone of control analysis and synthesis for single-input, single-output (SISO) systems since the seminal work of Bode [1] and Evans [2]. Along with the Nyquist plot [3], these techniques form the major part of what is commonly known as classical control methods. Three-dimensional (3-D) extensions of the classical Bode, Nyquist, and root locus plots have also been proposed [4], where the third dimension is either the frequency (in the Bode or Nyquist plots) or the gain (in root locus plots). The latter is called a gain plot in [4] and provides explicit information on the damping and frequency of the closed-loop eigenvalues as a function of the forward gain. An alternative extension of classical Bode analysis was introduced in the classical text on flight mechanics [5].

By Panagiotis Tsiotras

Specifically, in [5, pp. 112–153] the authors show the interrelationship between the root locus and frequency response diagrams. By adding a third dimension to the classical root locus plot (the gain) they show how this 3-D plot can be used to compute the location of the closed-loop roots as the intersection of paths of steepest descent with the corresponding contours of the logarithmic magnitude plot. Since this technique is not widely known and, to our knowledge, does not appear in standard undergraduate textbooks, the purpose of the present article is to revisit the generalized Bode diagram technique and demonstrate its usefulness for gaining a deeper understanding of both Bode and root locus analysis. Specifically, we provide additional insights on the connection between these two analysis methods, and we demonstrate this connection with several examples.

The Transfer Function and the Laplace Transform

The Bode and root locus methods work with the transfer function. The transfer function $G(s)$ of a system is defined as the ratio of the Laplace transform of the output to the Laplace transform of the input. In other words,

$$G(s) := \frac{Y(s)}{U(s)}, \quad (1)$$

where $Y(s) = \mathcal{L}[y(t)]$ and $U(s) = \mathcal{L}[u(t)]$ and $\mathcal{L}(\cdot)$ denotes the Laplace transform. Here $y(t)$ and $u(t)$, $t \geq 0$, are the output and input signals, respectively, of the forced (zero initial state) response. A consequence of (1) is the input-output relationship

$$Y(s) = G(s)U(s). \quad (2)$$

The Laplace transform of a function $f(t)$, $t \geq 0$, is defined by

$$F(s) = \mathcal{L}[f(t)] := \int_0^{\infty} f(t) e^{-st} dt. \quad (3)$$

Of course, for $F(s)$ to be well defined we need to make sure that the infinite integral in (3) exists. One way to ensure this existence is to impose the condition that the magnitude of the integrand becomes small for large values of the argument t . However, this condition may not be enough. For example, the integral from zero to infinity of $f(t) = 1/t$ does not exist. To make sure that the infinite integral in (3) exists, we need to ensure that its integrand becomes small *fast enough*. Exponential decay of the integrand in (3) is sufficient.

The role of the exponential term e^{-st} in the definition of the Laplace transform now becomes evident: Its purpose is to ensure that the integrand $f(t) e^{-st}$ decays to zero fast as $t \rightarrow \infty$. Since the function e^{-st} decays very quickly for large values of t whenever s has a positive real part, the Laplace transform can be defined for a large class of functions $f(t)$. Had we multiplied $f(t)$ with another function that did not decay fast enough as $t \rightarrow \infty$, the corresponding transform would be valid for very few functions. Such transforms do exist—the Hankel, Stieljes, and Mellin transforms are but a few examples [6]—but are not as widely used as the Laplace transform.

By far, however, the most important reason for the ubiquitous use of Laplace transforms in linear system theory is the property

$$\mathcal{L} \left[\int_0^t f(t-\tau)g(\tau) d\tau \right] = F(s)G(s), \quad (4)$$

where $F(s)$ and $G(s)$ are the Laplace transforms of the functions $f(t)$ and $g(t)$, respectively. Convolution in the time domain therefore corresponds to multiplication in the Laplace domain. The convolution integral in (4) arises in the solution of linear, time-invariant differential equations. For instance, the solution to the differential equation $\dot{x}(t) = ax(t) + u(t)$ with $x(0) = 0$ is given by

$$x(t) = \int_0^t e^{a(t-\tau)}u(\tau) d\tau.$$

Therefore, instead of solving differential equations in the time domain, we can solve *algebraic* equations in the Laplace domain!

Bode Plots

Let us now return to the input-output relationship (2). The first question one may ask is whether the transfer function defined in (1) is independent of the input $U(s)$. This property is not readily evident from (1), but it turns out to be the case for linear systems. In fact, the transfer function of a linear, time-invariant system is uniquely determined by the Laplace transform of the output response $y(t) = g(t)$ of the system to an impulse $u(t) = \delta(t)$, that is,

$$G(s) = \int_0^{\infty} g(t) e^{-st} dt.$$

Since s is, in general, a complex number, $G(s)$ is also a complex number. Let us denote its real and imaginary parts by G_x and G_y , respectively, so that $G(s) = G_x + iG_y$. The transfer function $G(s)$ can also be represented using polar (or phasor) notation as

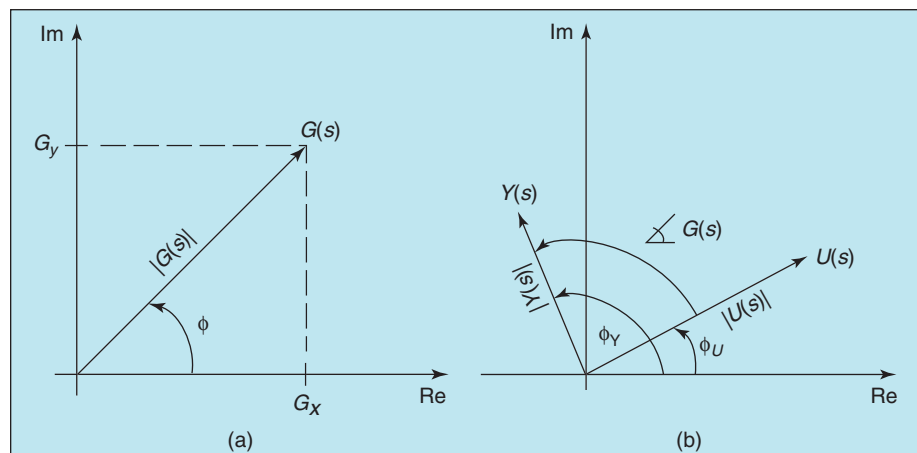


Figure 1. (a) Representation of $G(s) = G_x + iG_y$ in polar (phasor) form. The complex number $G(s)$ is also characterized by its magnitude $|G(s)|$ and angle $\phi = \angle G(s)$; (b) using this representation, the input and output are vectors rotating in the complex plane. Whether $Y(s)$ leads or lags $U(s)$ depends on the argument of $G(s)$.



Figure 2. A block diagram for a single-input, single-output system. The transfer function $G(s)$ is defined as the ratio of the Laplace transform of the output signal $Y(s)$ to the Laplace transform of the input signal $U(s)$. For linear time-invariant systems the transfer function $G(s)$ is independent of the choice of input $U(s)$.

$$G(s) = |G(s)| e^{i\phi}, \quad (5)$$

where $|G(s)| := \sqrt{G_x^2 + G_y^2}$ and $\phi = \angle G(s) := \arctan_2(G_y, G_x)$, where $-\pi \leq \arctan_2(G_y, G_x) \leq \pi$ is the four-quadrant inverse tangent of G_x and G_y ; see Figure 1(a).

The magnitude Bode diagram of a system with transfer function $G(s)$ provides information about the level of amplification of the input signal $U(s)$. Specifically, since the output is given by $Y(s) = G(s)U(s)$ (see also Figure 2), one obtains

$$|Y(s)| = |G(s)||U(s)|. \quad (6)$$

That is, the magnitude of the output is amplified (or attenuated) by the factor $|G(s)|$. By the same token, the angle (or phase) Bode diagram provides information about the relative angles of the signals $Y(s)$ and $U(s)$ in

the complex plane. This information is evident from the formula

$$\angle Y(s) = \angle G(s) + \angle U(s). \quad (7)$$

Notice that if $0 < \angle G(s) < \pi$, the output signal leads the input signal $U(s)$. Conversely, if $-\pi < \angle G(s) < 0$, then the output $Y(s)$ lags $U(s)$; see Figure 1(b).

Plots of $|G(s)|$ and $\angle G(s)$ as the complex variable $s = \sigma + i\omega$ varies along a path in the complex plane are called generalized Bode diagrams. The simplest case is to use straight lines in the s -plane. Generalized Bode diagrams are plots of $20 \log_{10}|G(s)|$ and $\angle G(s)$ versus $\log_{10}|s|$ when s varies along a straight line [5].

There are four types of generalized Bode diagrams that are used often [5, p. 135]. These diagrams correspond to four different paths in the complex plane, along which s is allowed to vary. If $s = i\omega$, that is, if s varies along the imaginary axis, we have the $i\omega$ -Bode diagram, or simply the Bode diagram. The second type is the σ -Bode diagram, in which $s = \pm\sigma$. In a σ -Bode diagram the variable s moves along the real axis. The third type of Bode diagram is the ζ -Bode diagram defined along the radial directions $s = |s|(-\zeta \pm i\sqrt{1-\zeta^2})$. Both the $i\omega$ -Bode diagram and the σ -Bode diagram are special cases of the ζ -Bode diagram. The former corresponds to the choice of $s = i\omega$, $\zeta = 0$, whereas the latter corresponds to the choice $s = \pm\sigma$, $\zeta = \pm 1$. The fourth type of Bode diagram is the shifted Bode diagram, in which the path of s is given by the line $s = \sigma_0 + i\omega$, where σ_0 is fixed. The paths of the shifted Bode diagram are therefore lines parallel to the imaginary axis.

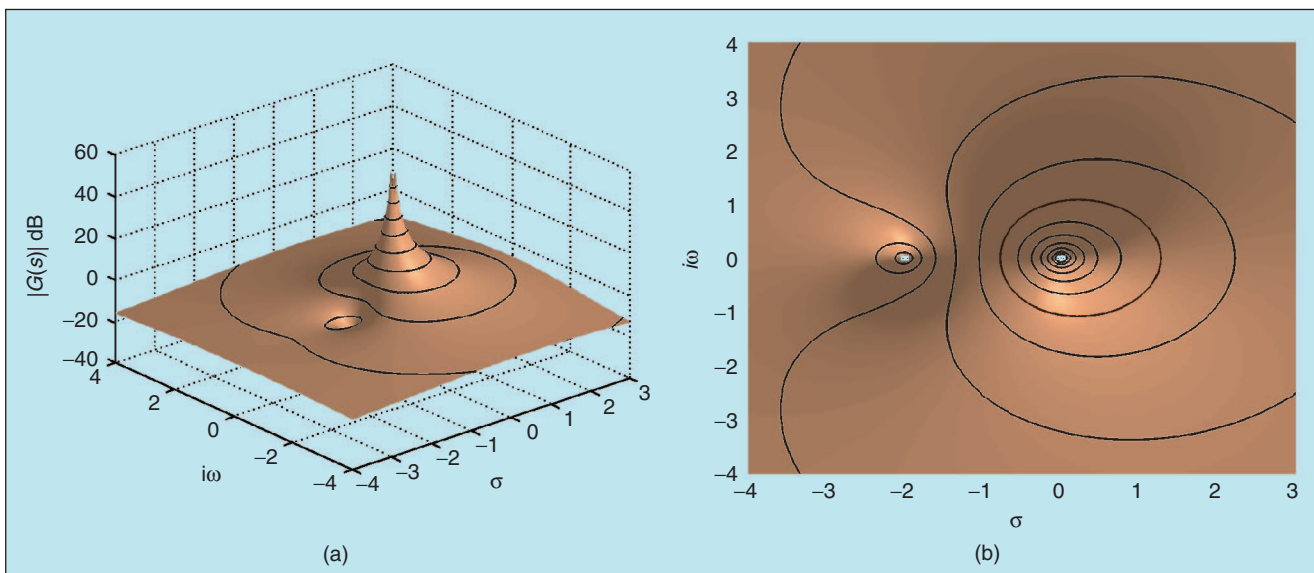


Figure 3. (a) The surface plot of the magnitude of the transfer function $G(s) = (s + 1)/s^2$ plotted in decibels. The peak is located at the pole, and the well is located at the zero. The solid dark lines are the contours of constant magnitude. (b) View of the surface from the top.

The 3-D Bode Diagram

Instead of computing a generalized Bode diagram for different choices of lines in the complex plane, we can compute the magnitude of $|G(s)|$ for all values of $s \in \mathbb{C}$ to obtain a surface $S(\sigma, \omega) = |G(s)|$, $s = \sigma + i\omega$ in the 3-D space. We call this the 3-D Bode diagram. For the rational transfer function

$$G(s) = \frac{\kappa (s + z_1)(s + z_2) \cdots (s + z_m)}{(s + p_1)(s + p_2) \cdots (s + p_n)}, \quad (8)$$

the surface $S(\sigma, \omega)$ has a collection of peaks and wells. In fact, assuming no pole/zero cancellations, all peaks are located at the poles p_1, p_2, \dots, p_n of $G(s)$ and all wells are located at the zeros z_1, z_2, \dots, z_m of $G(s)$. When plotting the magnitude of $G(s)$ on the logarithmic scale, all peaks and wells are infinitely high or infinitely deep, respectively, which can be seen by taking the logarithm of both sides of (8) to obtain

$$\log_{10} |G(s)| = \log_{10} |\kappa| + \sum_{i=1}^m \log_{10} |s + z_i| - \sum_{i=1}^n \log_{10} |s + p_i|. \quad (9)$$

Figure 3(a), for instance, shows the 3-D magnitude Bode diagram of the transfer function

$$G(s) = \frac{s+1}{s^2}. \quad (10)$$

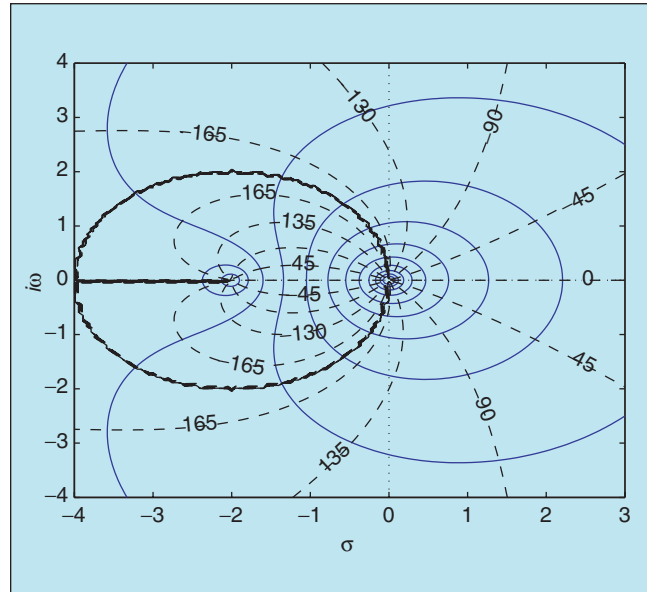


Figure 4. The isomagnitude (solid) and isophase (dashed) curves of the transfer function $G(s) = (s + 1)/s^2$ on the complex plane. The two sets of curves are perpendicular to each other. Stated differently, the isophase curves are always parallel to the local gradient of $|G(s)|$. By comparing with Figure 3(b) we see that these curves correspond to the view of the 3-D Bode diagram as seen from the top.

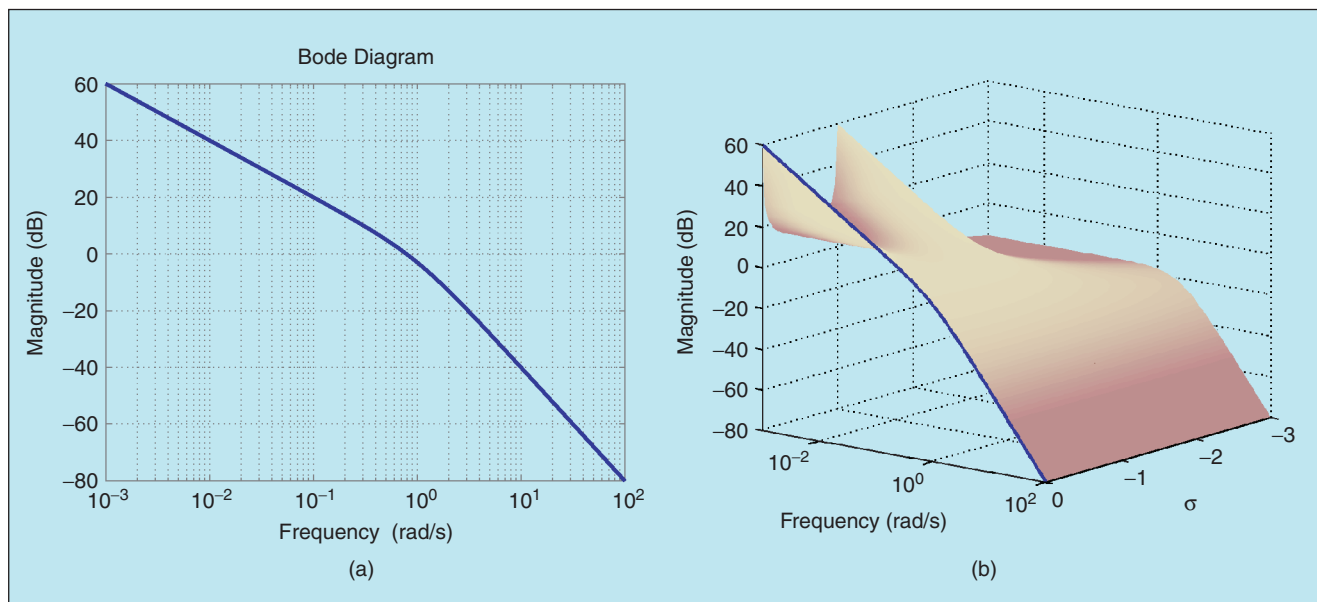


Figure 5. (a) Classical magnitude Bode diagram of the transfer function $G(s) = 1/[s(s + 1)]$. There is one corner frequency at $\omega_c = 1$ rad/s, corresponding to the pole $s = -1$. The mechanism by which the off-imaginary axis pole $s = -1$ influences the magnitude of $G(s)$ on the imaginary axis is revealed only by looking at the 3-D magnitude Bode diagram. (b) The 3-D magnitude Bode diagram of $G(s)$. The pole at $s = -1$ creates a uniform change in elevation. The change is felt on the imaginary axis at the corner frequency ω_c .

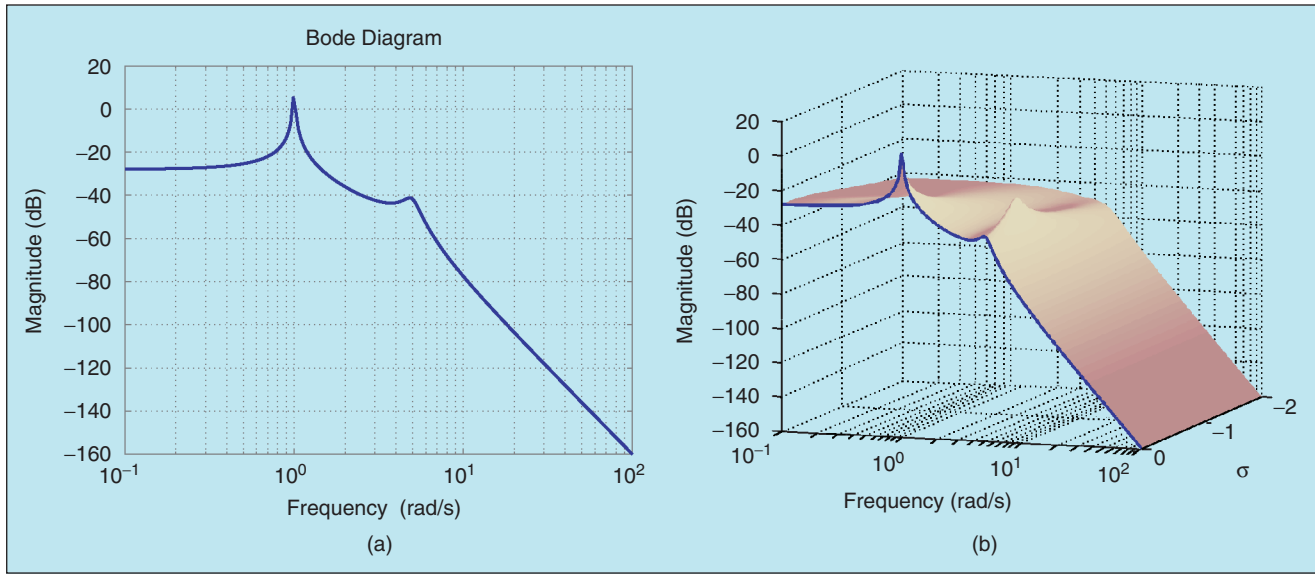


Figure 6. (a) Classical magnitude Bode diagram of the transfer function $G(s) = 1/[(s^2 + 1)(s^2 + s + 25)]$. There are two corner frequencies, namely, $\omega_{c1} = 1$ rad/s and $\omega_{c2} = 5$ rad/s. (b) The 3-D magnitude Bode diagram of $G(s)$. The pole at $s = -0.5 + i4.97$ creates a change in elevation. This change is felt on the imaginary axis at the corner frequency ω_{c2} . Notice that the larger the damping ratio, the farther away from the imaginary axis the pole is located and, hence, the less significant is this effect on the frequency axis.

A peak at $p = 0$ rises like a mountain over the landscape of $S(\sigma, \omega)$, and a bottomless well is located at the zero $z = -1$.

On this landscape we can draw the curves of constant magnitude of $G(s)$, that is, $|G(s)|_{\text{dB}} = \text{const}$. These are the *isomagnitude* curves of $G(s)$. The isomagnitude curves are shown as dark solid curves in Figure 3. When looking down from the positive vertical axis, we see the view shown in Figure 3(b). The isomagnitude curves now appear as precisely the level sets of the surface $S(\sigma, \omega)$.

We can also draw the constant-angle curves of $G(s)$, that is, $\angle G(s) = \text{const}$. These curves are the *isophase* or *isoargument* curves [5, pp. 112–115]. The isophase curves

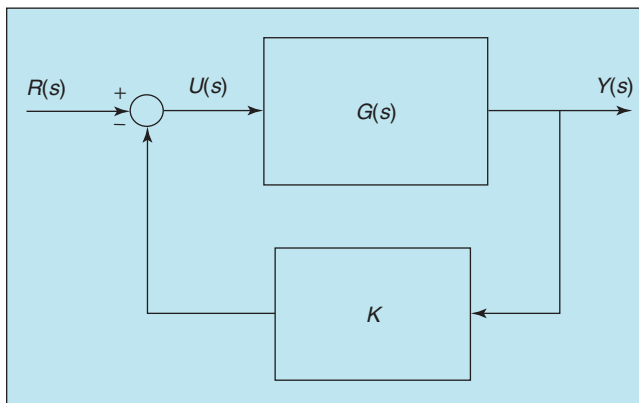


Figure 7. Block diagram of a closed-loop system with proportional feedback. Stability of the closed-loop system is determined by the location of the roots of the characteristic polynomial in the complex plane. The collection of the roots of the characteristic polynomial as K varies between zero and infinity comprises the root locus.

are shown as dotted lines in Figure 4. The isophase curves are perpendicular to the isomagnitude curves. To see why, recall from (5) that $G(s) = |G(s)|e^{i\phi}$. Therefore,

$$dG(s) = d|G(s)|e^{i\phi} + i d\phi|G(s)|e^{i\phi}. \quad (11)$$

Changes in $G(s)$ of constant magnitude correspond to $d|G(s)| = 0$ while isophase changes correspond to $d\phi = 0$. From (11) it follows that

$$dG(s) \Big|_{d|G(s)|=0} = i d\phi|G(s)|e^{i\phi} = d\phi|G(s)|e^{i(\phi+\frac{\pi}{2})} \quad (12)$$

and

$$dG(s) \Big|_{d\phi=0} = d|G(s)|e^{i\phi}. \quad (13)$$

The complex numbers $d\phi|G(s)|e^{i(\phi+\frac{\pi}{2})}$ and $d|G(s)|e^{i\phi}$ are perpendicular to each other since their arguments differ by $\pi/2$; see also Figure 1. As a result, isophase curves are normal to isomagnitude curves. Stated differently, the paths of constant angle of $G(s)$ are parallel to the gradient of $|G(s)|$ at each point. The orthogonality between the isophase and isomagnitude curves may also be inferred directly from the properties of the conformal mapping $s \mapsto G(s)$ [7, pp. 368–369]. The isophase curves of (10) are shown in Figure 4 along with the isomagnitude curves.

The 3-D magnitude Bode diagram also elucidates the effect of the off-imaginary axis poles and zeros on the magnitude of the classical Bode diagram. Recall that the classical

magnitude Bode diagram is the plot of $|G(i\omega)|_{\text{dB}}$ versus the frequency ω . Therefore, the classical magnitude Bode diagram looks at only a thin slice of the 3-D Bode diagram, namely the variation of the magnitude of the transfer function $G(s)$ along the imaginary (or frequency) axis. The traditional construction of the Bode diagram using graphical techniques, as taught in every undergraduate control textbook, instructs that corner points be introduced at each frequency, corresponding to a pole or zero of the transfer function, regardless of whether these poles or zeros are on the imaginary axis or not! These corner points modify the slope of the magnitude Bode diagram at each particular frequency. The corner points increase the slope by 20 dB/decade at each zero of the transfer function and decrease the slope by the same amount at each pole. What it is not at all clear from this construction, however, is why and how these off-imaginary poles/zeros have an effect on the magnitude of $G(s)$ on the imaginary axis.

Consider, for example, the transfer function

$$G(s) = \frac{1}{s(s+1)},$$

which has two poles, one of which is on the imaginary axis (actually, at the origin), and the other at $s = -1$. The magnitude Bode diagram of this transfer function is shown in Figure 5(a). The slope is -20 dB/decade up to the cor-

ner frequency $\omega_c = 1$ rad/s. After that, the slope decreases to -40 dB/decade. But how does the pole at $s = -1$ affect the slope of the classical Bode diagram on the imaginary axis for frequencies larger than ω_c ?

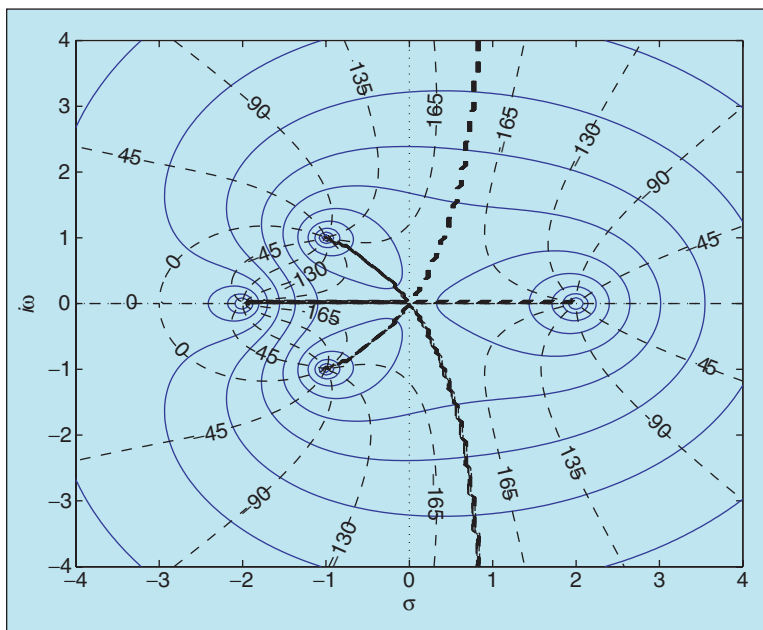


Figure 8. The isomagnitude (solid) and isophase (dashed) curves of the transfer function $G(s) = (s + 1)/[(s^2 + 2s + 1)(s - 2)]$. The two sets of curves are perpendicular to each other. The root locus follows the isophase curves that satisfy the condition $\angle G(s) = 180^\circ \pm k360^\circ$, $k = 0, \pm 1, \pm 2, \dots$. The root locus is shown by a thicker line. This root locus has the unusual property that three poles meet at the origin, forming a so-called triple point.

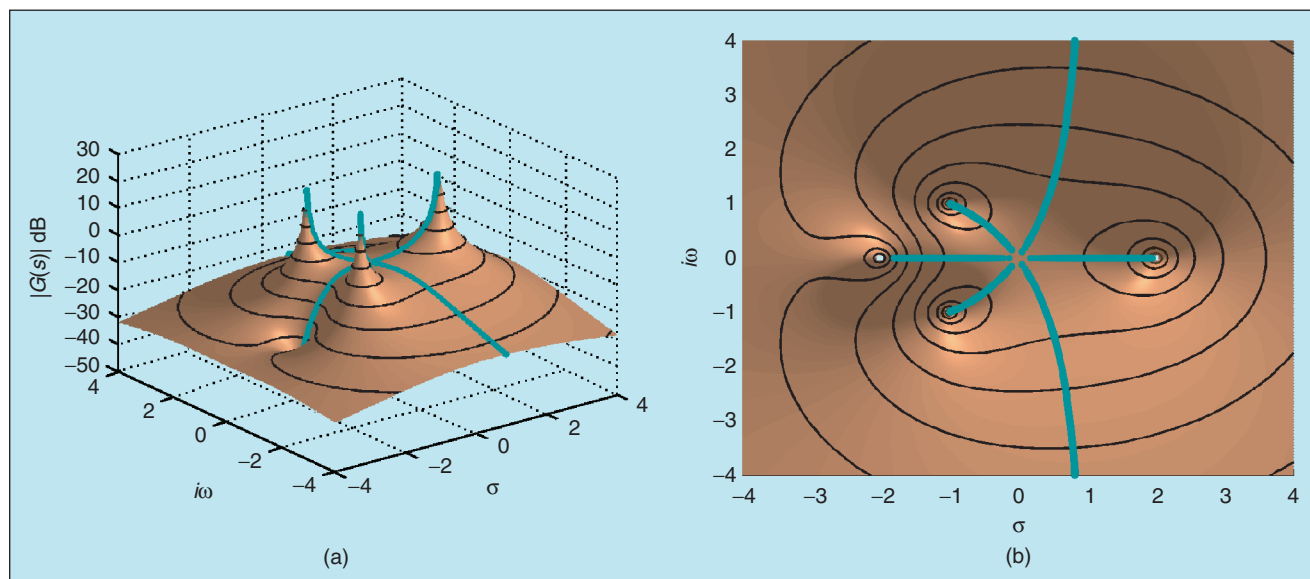


Figure 9. (a) The 3-D magnitude Bode diagram (in dB) of $G(s) = (s + 1)/[(s^2 + 2s + 1)(s - 2)]$. The peaks correspond to the poles, and the wells correspond to the zeros. The green line shows the path to be followed by a ball released from one of the peaks. This path corresponds to steepest descent. (b) View from the top. The path traced by the ball is the root locus; compare with Figure 8.

The 3-D Bode diagram, shown in Figure 5(b), reveals the hidden connection. The pole at $s = -1$ changes the elevation of the 3-D Bode landscape. This change in elevation is uniform in every direction around the point $s = -1$. The

effect of this change in elevation is felt on the imaginary axis at exactly the corner frequency $\omega_c = 1$ rad/s. Each pole or zero changes the elevation of the whole landscape, and its influence is felt at the corresponding frequency on the imaginary axis.

A second example is shown in Figure 6, where the classical Bode diagram and the 3-D magnitude Bode diagram of the transfer function

$$G(s) = \frac{1}{(s^2 + 1)(s^2 + s + 25)}$$

are depicted. This transfer function has a purely imaginary pair of poles at $s_{1,2} = \pm i$ and another complex pair at $s_{3,4} = -0.5 \pm i 4.97$. The corner frequencies are at $\omega_{c1} = 1$ rad/s and $\omega_{c2} = 5$ rad/s. The pole at $s = -0.5 + i 4.97$, although not on the imaginary axis, creates a change in the elevation of the 3-D Bode magnitude landscape. This change is felt on the imaginary axis at the corner frequency ω_{c2} . Moreover, the damping ratio ζ of the pole plays a significant role in the shape of the frequency response around the corner frequency. The larger the damping ratio, the farther away from the imaginary axis (for the same frequency) the pole will be and hence the less significant the effect of the pole on the imaginary

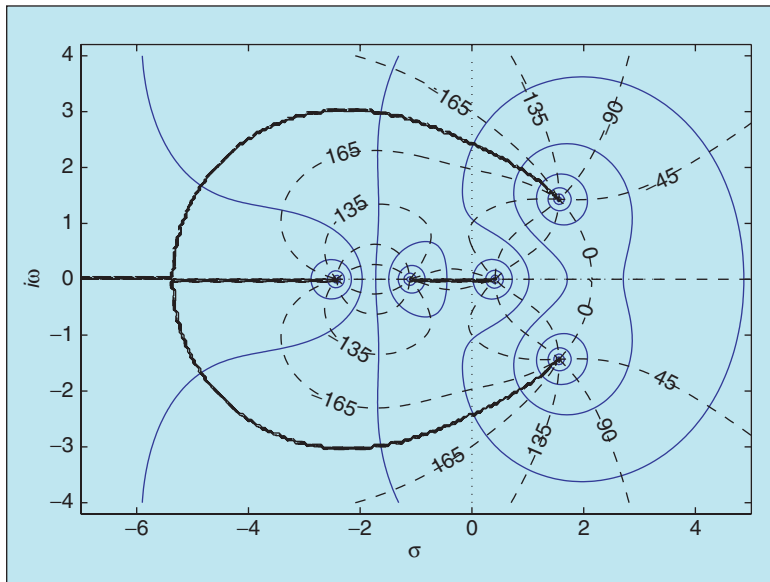


Figure 10. The isomagnitude (solid) and isophase (dashed) curves of the transfer function $G(s) = (s^2 + 2s - 1)/(s^3 - 2s^2 + s + 5)$. The two sets of curves are perpendicular to each other. The root locus follows the isophase curves that satisfy the condition $\angle G(s) = 180^\circ \pm k360^\circ$, $k = 0, \pm 1, \pm 2, \dots$. The root locus is shown by a thicker line.

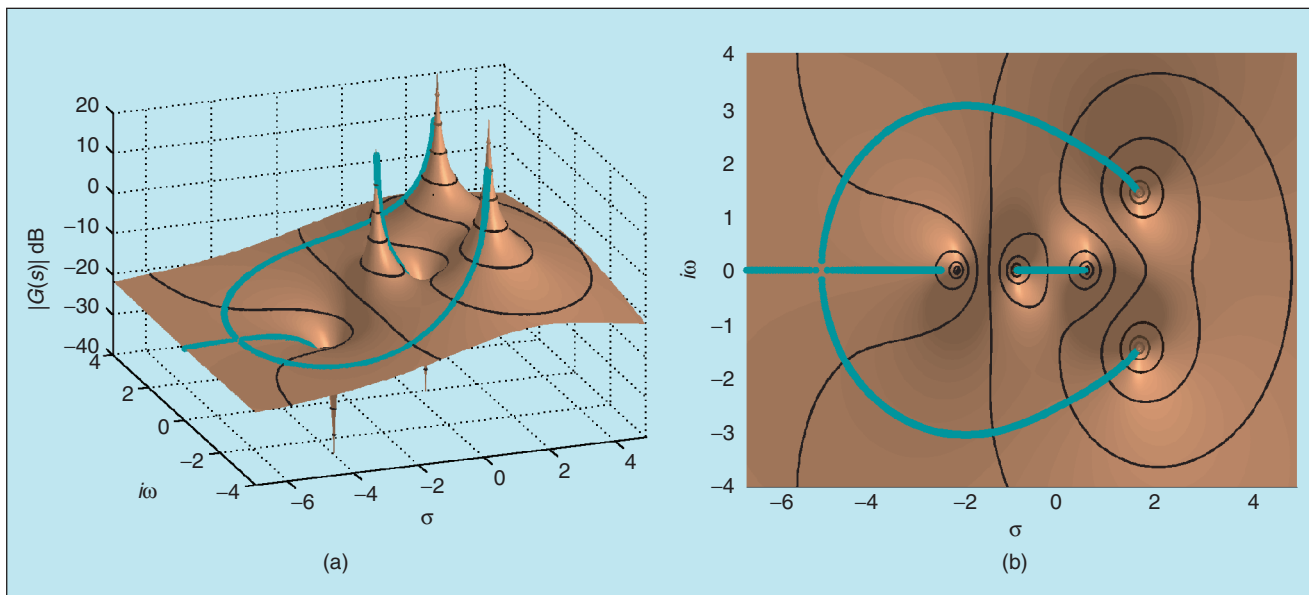


Figure 11. (a) The 3-D magnitude Bode diagram (in decibels) of $G(s) = (s^2 + 2s - 1)/(s^3 - 2s^2 + s + 5)$. The peaks correspond to the poles, and the wells correspond to the zeros. The green line shows the path to be followed by a ball released from each of the peaks. This path corresponds to steepest descent. This example has three poles and two zeros. If three balls are released simultaneously, the ball released from $p = -1.1163$ rolls directly into the well at $z = -1 + \sqrt{2}$, while the other two collide at $s = -5.3561$, with one of them rolling into the second well at $z = -1 - \sqrt{2}$, and the other ball rolling to infinity along the negative real axis. (b) View from the top. The path traced by the balls is the root locus, which is shown in Figure 10.

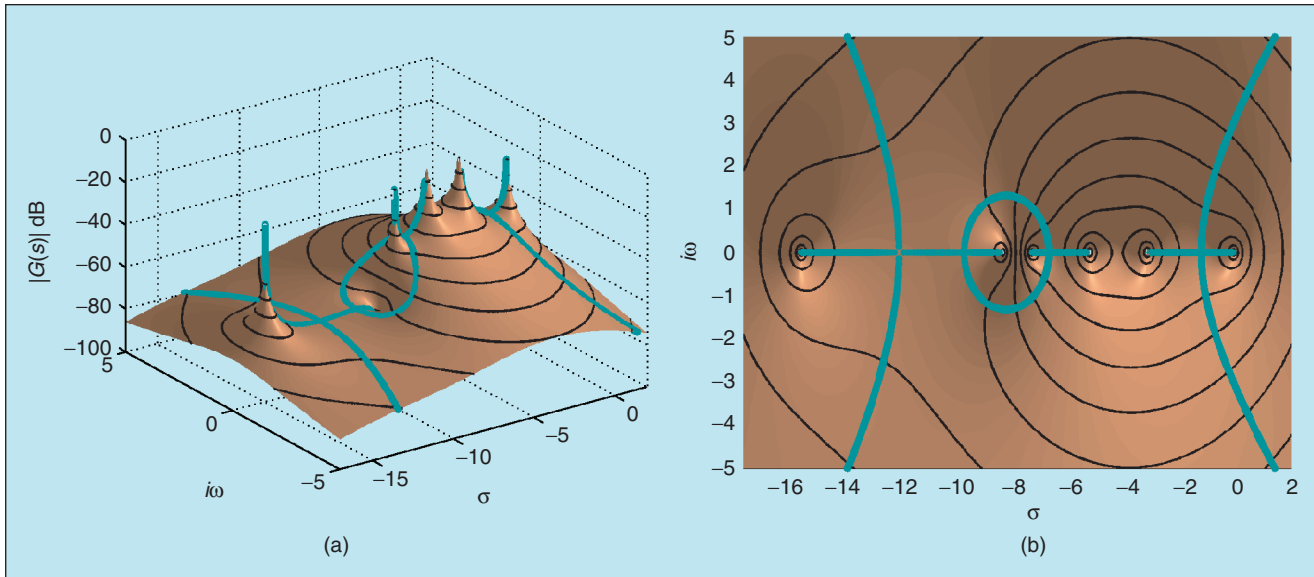


Figure 12. (a) The 3-D magnitude Bode diagram (in decibels) of $G(s) = (s + 8)/[(s + 15)(s + 7)(s + 5)(s + 3)s]$. Here there are four more peaks than wells. The paths of five balls released simultaneously from the five peaks are shown in green. Since there is only one well, four of the five balls roll down the slopes of the surface to infinity. (b) View from the top. The paths traced by the balls form the branches of the root locus, which is shown in Figure 13.

axis (that is, the frequency response) will be; see Figure 6(b).

We therefore see that the 3-D magnitude Bode diagram provides a wealth of information about the behavior of the transfer function, which is not directly evident by looking at its magnitude only along the frequency axis. The 3-D magnitude Bode diagram is also intimately connected with the other classical control design technique, that is, the root locus. This connection is unraveled next.

The Locus of the Roots

Given the SISO plant with transfer function $G(s)$, the feedback control $u = -Ky + r$ yields the closed-loop system shown in Figure 7. The closed-loop transfer function $G_{CL}(s)$ for the system in Figure 7 is given by

$$G_{CL}(s) = \frac{G(s)}{1 + KG(s)}.$$

The poles of $G_{CL}(s)$ are given by the roots of the characteristic equation

$$1 + KG(s) = 0. \quad (14)$$

These poles depend on the value of the feedback gain K . As the scalar K varies from zero to infinity the roots of (14) follow a path in the complex plane, called the root locus. A simple argument shows that all of roots of (14) start at the

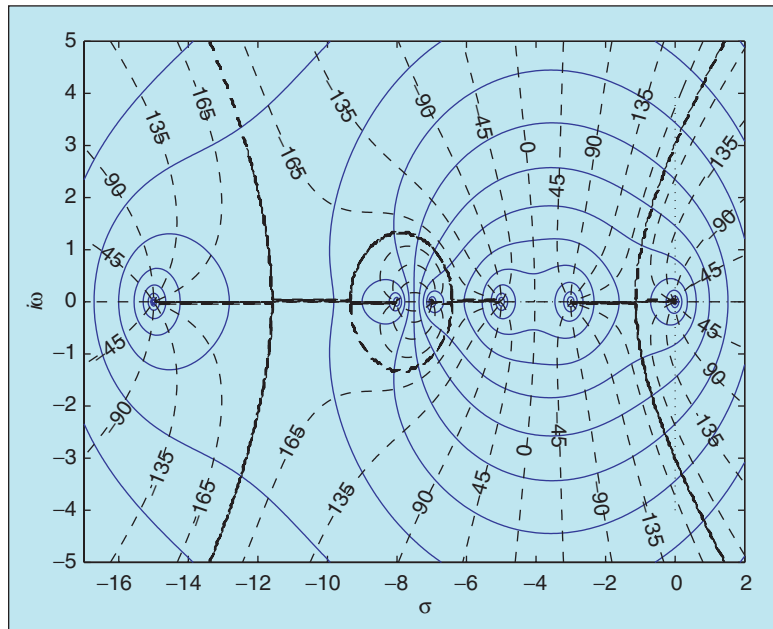


Figure 13. The isomagnitude (solid) and isophase (dashed) curves of the transfer function $G(s) = (s + 8)/[(s + 15)(s + 7)(s + 5)(s + 3)s]$. The root locus is shown by a thicker line. There are several branches, four of which escape to infinity.

poles of $G(s)$ for $K = 0$, and converge to the zeros of $G(s)$ or to infinity along certain directions as $K \rightarrow \infty$.

Equation (14) implies that $KG(s) = -1$ and therefore

$$\angle G(s) = 180^\circ \pm k360^\circ, \quad k = 0, \pm 1, \pm 2, \dots \quad (15)$$

The root locus path is therefore along isophase curves of $G(s)$, namely, those given in (15). As shown before, isophase curves are normal to the level sets of $|G(s)|$. Since the roots start from the poles and end up at the zeros of $G(s)$ (or at infinity), the branches of the root loci are paths of steepest descent (that is, negative of the gradient) of $|G(s)|$.

This observation invites a nice interpretation of the root locus paths on the surface of the 3-D Bode diagram. Since these are paths of steepest descent they can be visualized as the paths traced by a ball released from the top of each peak (pole). The ball slides down the slope of the peak towards a well (zero). The projection of this path on the $\sigma - \omega$ plane is exactly the classical (two-dimensional) root locus on the complex plane.

Numerical Examples

Example 1

Consider the transfer function

$$G(s) = \frac{s+1}{(s^2+2s+1)(s-2)}, \quad (16)$$

which has three peaks, located at the poles $p_{1,2} = -1 \pm i$, $p_3 = 2$, and one well located at $z_1 = -1$. Figure 8 shows the level curves of $|G(s)|$ on the complex plane along with the isophase curves. The 3-D surface of $|G(s)|_{\text{dB}}$ and the corresponding root locus paths are shown in Figure 9(a). Figure 9(b) shows the view from the top. Comparing with Figure 8 we see that these paths coincide with the classical root locus plot.

Example 2

Consider the transfer function

$$G(s) = \frac{s^2+2s-1}{s^3-2s^2+s+5}. \quad (17)$$

This transfer function has two zeros located at $z_{1,2} = -1 \pm \sqrt{2}$ and three poles located at $p_{1,2} = -1.5582 \pm i1.4321$ and $p_3 = -1.1163$. Figure 10 shows the level curves of $|G(s)|$ along with the isophase curves. The 3-D surface of $|G(s)|_{\text{dB}}$ and the corresponding root locus path are shown in Figure 11(a). Figure 11(b) shows the view from the top.

Example 3

Consider the transfer function

$$G(s) = \frac{s+8}{(s+15)(s+7)(s+5)(s+3)s}. \quad (18)$$

The 3-D Bode surface plot along with the paths of steepest descent are shown in Figure 12. This example has the rather interesting root locus shown in Figure 13. Since

there are four more poles than zeros, there are four branches in the root locus that escape to infinity.

Conclusions

We have shown that there is a close connection between the classical magnitude Bode diagram and the root locus plot. The magnitude Bode diagram creates a 3-D landscape of peaks and wells in the complex plane, and the root locus consists of the paths of steepest descent from the peaks to the wells in this landscape.

Although Bode diagrams and root locus plots have been at the forefront of control system education, their relation does not seem to be widely known. In fact, this link between Bode and root locus plots is unfortunately missing from virtually all undergraduate control textbooks. The purpose of this short note is to bring this connection into new light, and provide an incentive to educators to delve deeper into the seminal work of the pioneers in the field, since there is more to classical control theory than meets the eye.

References

- [1] H.W. Bode, *Network Analysis and Feedback Amplifier Design*. New York: Van Nostrand, 1945.
- [2] W.R. Evans, "Graphical analysis of control systems," *Trans. Amer. Inst. Electr. Eng.*, vol. 67, pp. 547-551, 1948.
- [3] H. Nyquist, "Regeneration theory," *Bell Syst. Tech. J.*, vol. 11, pp. 126-147, 1932.
- [4] T.R. Kurfess and M.L. Nagurka, "Geometric links among classical control tools," *IEEE Trans. Educ.*, vol. 37, no. 1, pp. 77-83, 1994.
- [5] D. McRuer, I. Ashkenas, and D. Graham, *Aircraft Dynamics and Automatic Control*. Princeton, NJ: Princeton Univ. Press, 1973.
- [6] N. Bleistein and R.A. Handelsman, *Asymptotic Expansions of Integrals*. New York: Dover, 1986.
- [7] K. Ogata, *Modern Control Engineering*, 4th ed. Upper Saddle River, NJ: Prentice Hall, 2002.

Panagiotis Tsiotras (p.tsiotras@ae.gatech.edu) is associate professor in the School of Aerospace Engineering at the Georgia Institute of Technology. From 1994-1998 he was an assistant professor with the Department of Mechanical and Aerospace Engineering at the University of Virginia. He holds degrees in aerospace engineering (Ph.D., Purdue, 1993, MS, Virginia Tech. 1987), mathematics (MS, Purdue, 1992) and mechanical engineering (Eng. Dipl., NTUA, Athens, Greece, 1986). He is associate editor of *AIAA Journal of Guidance, Control, and Dynamics* and *IEEE Control Systems Magazine*, and past associate editor of *Dynamics and Control*. He is an Associate Fellow of AIAA and a Senior Member of IEEE. His research interests include dynamics and control of nonlinear systems, and optimal and robust control with applications to aerospace, mechanical, and biological systems. He can be contacted at the School of Aerospace Engineering, Georgia Institute of Technology, Atlanta, GA 30332-0150 USA.

